

Band engineering in graphene with superlattices of substitutional defects

Simone Casolo^a, Rocco Martinazzo^{a,b}, Gian Franco Tantardini^{a,b*}

^a*Dipartimento di Chimica Fisica ed Elettrochimica,*

Università degli Studi di Milano, via Golgi 19, 20133 Milan, Italy.

^b*CIMAINA, Interdisciplinary Center of Nanostructured Materials and Interfaces, Milan, Italy.*

We investigate graphene superlattices of nitrogen and boron substitutional defects and by using symmetry arguments and electronic structure calculations we show how such superlattices can be used to modify graphene band structure. Specifically, depending on the superlattice symmetry, the structures considered here can either preserve the Dirac cones (D_{6h} superlattices) or open a band gap (D_{3h}). Relevant band parameters (carriers effective masses, group velocities and gaps, when present) are found to depend on the superlattice constant n as $1/n^p$ where p is in the range $1 - 2$, depending on the case considered. Overall, the results presented here show how one can tune the graphene band structure to a great extent by modifying few superlattice parameters.

I. INTRODUCTION

Single layer graphene is a very promising material for a future silicon-free nanoelectronics. The peculiar character of its charge carriers comes from the intersection of the π/π^* electronic bands occurring at the corners of its hexagonal Brillouin zone. This gives rise to the so-called Dirac cones at the Fermi level and makes graphene a zero-gap semiconductor¹ in which low energy excitations behave as massless, chiral Dirac particles^{2,3}. In turn, this implies a series of interesting physical effects that open new perspectives for fabricating novel electronic devices⁴, *e.g.* high-performance transistors for radiofrequency applications^{5,6}. In this perspective the possibility of engineering graphene's band structure by introducing defects, strains or external potentials has gained importance in the recent past, in particular for opening a gap in the band structure which is essential to design logic devices. Indeed the non-vanishing residual conductance of intrinsic graphene avoids the complete current pinch-off in the pristine material^{7,8}, thereby limiting the on-off ratio to $\sim 10^1 - 10^2$. A number of controlled techniques for energy band engineering have been proposed other than the actively pursued goal to obtain nanoribbons of controlled size and edge geometry. Most of them are based on the use of superlattices of external potentials^{9,10} or defects such as holes^{11,12} and adsorbates¹³. Controlled vacancies on graphene¹⁴, as well as large holes symmetrically arranged to form graphene anti-dots¹⁵ have actually been realized with modern lithographic and self-assembling techniques. Preferential sticking of atoms induced by Moiré patterns¹⁶ or by other electronic effects^{17,18} could also induce a superlattice ordering that modifies graphene energy bands. Likewise, there is a great hope that novel bottom-up techniques¹⁹ may be applied to fabricate atomically precise graphenic structures as already shown for nanoribbons²⁰. These approaches might allow to realize in the near future graphene-related two-dimensional materials with *modified* characteristics, *e.g.* linearly-dispersing bands with variable Fermi velocities or semiconducting structures. In this paper we focus on atomically precise superlattices of substitutional

atoms. The present work connects to and extend a recent work²¹ where we have shown that in properly designed superlattices of holes or adatoms one can open a gap *without* breaking graphene point symmetry, *i.e.* preserving the pseudo-relativistic behaviour of charge carriers which makes graphene so attractive. The structures suggested in Ref.²¹ have π vacancies (hence missing p_z orbitals) at the sites of a honeycomb superlattice, as a consequence of the introduction of C vacancies (holes) or chemisorption of simple atomic species. Here we consider similar, highly symmetric structures, but with π vacancies replaced by boron and nitrogen. Similar defects have been recently considered for tuning the electronic properties of graphene nanoribbons and other carbon based structures suggesting that, when arranged to form particular structures, they can turn the material into a semiconductor or a half-metal²²⁻²⁴. Half-metallicity and the other many-body effects in such a structures open new perspectives in the field of carbon-based materials for spintronic applications: for a recent review see Ref.^{25,26} and references therein.

In this paper we show that, depending on the superlattice symmetry, one can obtain either electron (hole) doped substrates with pseudo-relativistic massless carriers or semiconducting structures with a quasi-conical dispersion, and with the help of electronic structure calculations (tight-binding and density-functional theory) we determine carriers velocities, effective masses and band gaps (when present) as functions of the superlattice. The focus is on boron and nitrogen, mainly because of the fast progresses in methods for the controlled synthesis of B and N doped graphenes. For instance, Panchakarla *et al.*²⁷ have recently shown how it is possible to insert B or N dopants in graphene by adding the correct precursors in the arc discharge chamber, while Ci *et al.*²⁸ have reported the synthesis of large islands of boron nitride embedded in graphene by atomic layer deposition techniques. Methods to selectively replace C atoms in the graphene lattice have also been proposed²⁹, thereby suggesting that the superlattice structures considered in this paper might soon become feasible.

The paper is organized as follows. In the next section we summarize the computational details of the calculations.

Table I: Parameters used in the tight-binding Hamiltonian. All the values are in eV.

Atom	ϵ	t_1	t_2	t_3
C	0.000	-2.900	+0.175	-0.155
B	-1.5225	+1.450	-	-
N	+1.5225	-1.450	-	-

Then, we show how p -(n -) doped graphene-like structures result when substitutional defects are arranged in *honeycomb* superlattices, whereas semiconducting structures with quasi-conical dispersion (massive Dirac carriers) result either from a *hexagonal* superlattice or from a honeycomb co-doped superlattice. Finally, we summarize and conclude.

Throughout this paper we define the superlattice periodicity using Wood's notation, *i.e.* by multiplying graphene's two-dimensional lattice vectors by the integer (superlattice) constant n .

II. COMPUTATIONAL METHODS

The results shown in the next sections have been obtained from both tight-binding (TB) and density functional theory (DFT) electronic structure calculations. In the first case we diagonalized the usual tight-binding Hamiltonian for graphene $\pi - \pi^*$ system, applying periodic boundary conditions and including hopping terms up to the third nearest-neighbors. The on-site energies ϵ_i and hopping terms t_1 , t_2 and t_3 (for nearest, next-to-nearest and next-to-next-nearest neighbors, respectively) are those proposed by Nanda *et al.*³⁰. They were fitted to accurate all-electron calculations to correctly reproduce the Fermi velocity of single layer graphene. For the dopant atoms we only considered hoppings to nearest neighbor sites. Their values (t_1), as well as those of the on-site energies (ϵ_i), are those introduced by Peres *et al.*³¹, who have already successfully used them to study electronic effects in doped graphene. A summary of the TB parameters is listed in I.

First principles DFT calculations were performed with the help of the VASP suite^{32,33}, using a supercell approach. Core electrons were taken into account by projector augmented wave (PAW) pseudo-potentials while for valence a 500 eV plane wave cutoff was used. To correctly represent the defect induced charge inhomogeneities we used the Perdew-Burke-Ernzerhof (PBE) gradient-dependent exchange and correlation functional³⁴. Band structures were sampled by a Γ centered k -points grid, never sparser than 6x6x1 in order to include every special point in the Brillouin zone (BZ).

The TB parametrization was tested by comparing the band structure of few superlattices along the Γ -K-M-K'- Γ path with accurate DFT results. In every case the adopted parametrization was found to be accurate

enough to reproduce the bands close to the Fermi energy.

Therefore, we computed DFT band structures for nxn graphene superlattices up to $n=14$, and for larger structures we relied on TB calculations only.

III. RESULTS AND DISCUSSION

Graphene's peculiar electronic structure is strictly related to the point symmetry of its lattice, D_{6h} in the Shönflies notation. In the Brillouin zone, for each Bloch electronic state with k vector \mathbf{k} , the relevant symmetry elements are those which either leaves \mathbf{k} invariant or transforms it into one of its equivalent images, *i.e.* $\mathbf{k} \rightarrow \mathbf{k} + \mathbf{G}$ being \mathbf{G} a reciprocal lattice vector. These elements form a subgroup of D_{6h} , known as little co-group or simply k -group at \mathbf{k} ³⁵, which determines the possible symmetries of the electronic states at \mathbf{k} . At the high symmetry point K (or K') of graphene's Brillouin zone the k -group is D_{3h} , and Bloch functions built as linear combinations of p_z orbitals span a two-dimensional irreducible representation (irrep) of such a symmetry group (E''). This is enough for the $\pi - \pi^*$ degeneracy and the unusual linear dispersion at K (K'). That this occurs exactly at the Fermi level is a consequence of the electron-hole ($e - h$) symmetry which approximately holds in graphene. Indeed, thanks to this extra symmetry, energy levels are always symmetrically arranged and, at half-filling, the Fermi level lies exactly at the center of the spectrum, where any doubly degenerate level is forced to lay⁵³. In general, the number of doubly degenerate irreps in the BZ determines alone the presence of states (absence of a gap) at the Fermi level. We have recently shown²¹ how one can turn such number to be even at every special point -thus opening a gap in the band structure- by symmetrically removing " p_z orbitals" in forming certain nxn superlattices. Substitutional defects behave similarly to p_z vacancies (to which they reduce when the hoppings become zero) but introduce impurity bands which partially hybridize with those of the substrate. In addition, the diagonal disorder they introduce breaks $e - h$ symmetry giving rise to a Fermi level shift, *i.e.* to p - and n - doping for group IIIA and VA elements, respectively, as recently shown for both graphene³⁶ and nanotubes³⁷. In the weakly defective superstructures considered in the following the defect-induced perturbation affects the electronic structure close to the Fermi level. With homogeneous doping the latter shifts at most proportionally to $1/n$, *i.e.* as the square root of the defect concentration, as a consequence of the linear-energy dispersion which implies $E_F = v_F \sqrt{\pi n_e}$, where v_F is the Fermi velocity of pristine graphene and n_e is the electron (hole) excess density, $n_e \propto 1/n^2$. Hence, analogously to the superlattices of p_z vacancies²¹, we make use of symmetry arguments to establish whether degeneracy occurs at the BZ special points in the important low-energy region. It is worth noticing at this point that, however small

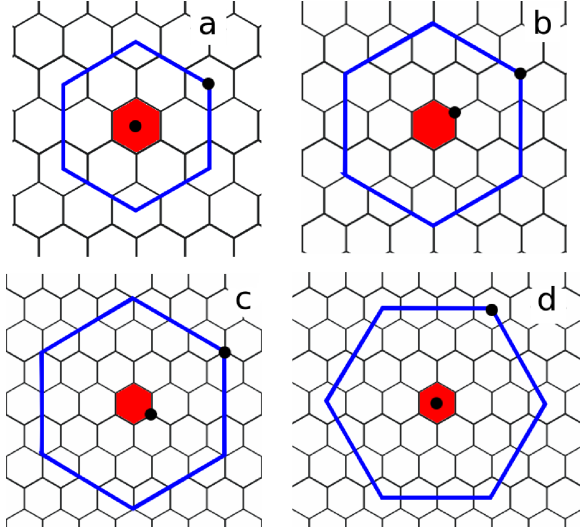


Figure 1: Folding of graphene Brillouin zone (BZ, blue line) into the superlattice ones (red filled hexagon) for some nxn structures, a) $n=3m$, b) $n=3m+1$ and c) $n=3m+2$, along with the case of $\sqrt{3}nx\sqrt{3}nR30^\circ$ superlattices (d). The K point in graphene's BZ, is labeled with a black filled dot.

the defect perturbation is, the folding of graphene band structure occurs differently according whether the superlattice constant n belongs to the sequence $n = 3m$ or $n = 3m + 1, 3m + 2$ (m integer). As shown in 1 for the superlattices considered in this work (a-c), for $n = 3m + 1$ ($3m + 2$) K and K' fold separately into $K_n(K'_n)$ and $K'_n(K_n)$, whereas for $n = 3m$ they both fold to the BZ center Γ_n . This means that $n = 3m$ superlattices are expected to have rather unique properties related to the highly degenerate nature of the unperturbed spectrum. In the following we mainly focus on $n = 3m + 1, 3m + 2$ superlattices and only occasionally look at the properties of $n = 3m$ ones. A further six-fold superlattice symmetry, the $\sqrt{3}nx\sqrt{3}nR30^\circ$ case reported in 1(d), will not be considered here since in that case band folding occurs analogously to the $3m \times 3m$ case discussed above.

A. Honeycomb superlattices

A honeycomb-shaped superlattice is a natural choice for nxn superlattices (nxn -honeycombs thereafter), since it preserves the D_{6h} point group symmetry of pristine graphene. The superlattice unit cell contains two substitutional atoms and is shown in 2. If the atomic radii of the dopants are small enough that lattice distortions are minimal, the system overall symmetry is preserved and Dirac cones at K_n and K'_n are expected. This is the case of boron and nitrogen substitutional defects, whose DFT-optimized structures show no appreciable lattice distortion. Both TB and DFT calculations confirm that $n = 3m + 1$ and $3m + 2$ honeycomb superlattices made of B or N substitutional defects only show a

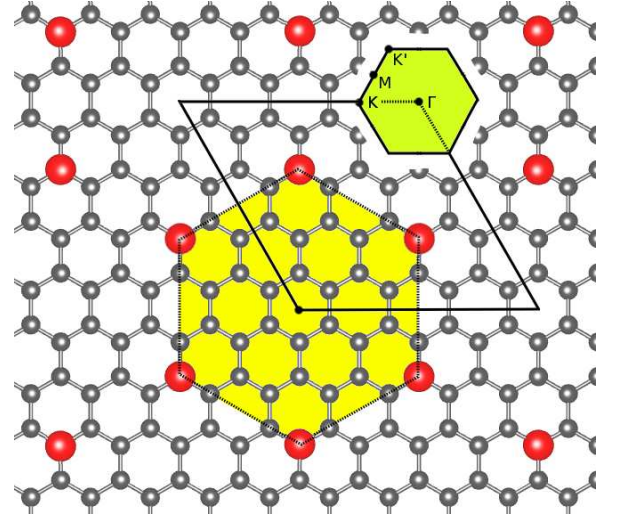


Figure 2: A 4×4 -honeycomb superlattice: the black line represents the unit cell while the Wigner-Seitz and Brillouin zone are shown in yellow and green respectively. Red balls are sublattice substitutional defects forming the superlattice.

low-energy band structure very similar to that of perfect graphene, but with the Fermi level lying respectively below (p -doped) and above (n -doped) their Dirac point. In principle, with properly designed n - or p - back-doping, *e.g.* electric-field induced but also *via* molecular adsorption^{38,39}, such shift can be offset and the analogy with pristine graphene can be fully exploited.

3(a) shows the TB and *first principles* band structures of one nxn -honeycomb together with the position of the Fermi level (3(c)) in such n - and p -doped superlattices at different impurity concentrations. As expected, the shift (Δ) of the Dirac cones with respect to the Fermi level (see 3(c)) is, to a good approximation, inversely proportional to the dopant concentration for both B and N doping, though with opposite sign. The difference between TB and DFT band structure is minimal, and this confirms that the tight binding parameters adopted are good enough for accurately describing the low-energy features of the nxn -honeycomb superlattices investigated in this paper. In 3(b) we also report the unique band structure resulting from the special folding in the $n = 3m$ sequence; as it is evident from the inset of 3(b), the four-fold degeneracy occurring at Γ_n is partially lifted, and a gap is introduced in one of the two cone replica.

The group velocity for electrons and holes taken close to the cone apex (but rather adequate for a wider energy range) is shown in 3(d) for n - and p -doped superlattices. The two curves approach the limit of clean graphene with different trends. Upon non-linear curve fitting the group velocity v (relative to the one in pristine graphene) for p -doped honeycombs is found to behave as $v/v_F \propto 1 - n^{-1.29}$, while for n -doped honeycombs as $\propto 1 - n^{-1.84}$. The difference between the two cases is due to the value of the on-site energies and hopping of the dopants which determine the degree of hybridization of

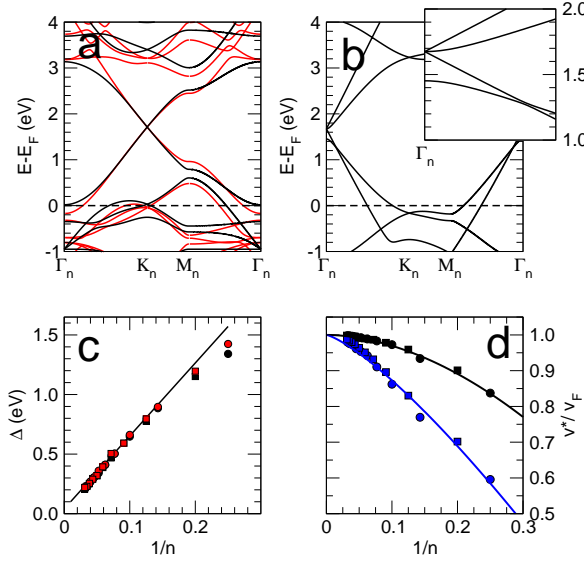


Figure 3: *a*): TB (black lines) and DFT (red lines) band structures for the 4x4-honeycomb boron superlattice. *b*) the TB band structure of the 3x3-honeycomb boron superlattice arising from folding in $n = 3m$ superlattices. The inset shows a close-up of the region close to Γ_n . *c*) Absolute shift of the Dirac cones apex (Δ) with respect to the Fermi level, in p -doped (B, red) and, n -doped (N, black) honeycombs. *d*) Group velocity for charge carriers close to the cones apex for the boron (black) and nitrogen (blue) case. Circles and squares for $n = 3m + 1$ and $n = 3m + 2$.

their impurity levels with that of bulk graphene. With the parameters used (see I), which are symmetric with respect to the on-site energy of C atoms, this can only happen because of the asymmetry in graphene electronic structure introduced by the next-to-nearest neighbor interactions. Other superlattices made of group IIIA (Al, Ga, In) and VA (P, As, Sb) dopants have been tested by *first principles* calculations. In any case we found that, after geometric optimization of the lattice structure, the impurities stand out from the graphene layer plane and considerably distort the neighboring lattice positions. The resulting band structures are metallic but lack of Dirac cones due to the reduced symmetry.

B. Hexagonal superlattices

When one defect per supercell only is introduced a nxn hexagonal superlattice (a “ nxn -hexagon”) results, as shown in 4. This kind of structures is closely related to the honeycomb ones, having one extra substitutional atom at the center of a hexagon of defects. A closer inspection, however, reveals that, due to the presence of the underlying C network, the point symmetry is reduced to D_{3h} , with σ planes missing with respect to the honeycomb counterparts. It follows that the k -group at K_n (K'_n) is C_{3h} , with no irreducible two-dimensional (complex) representations (see 5). Hence, degeneracy is re-

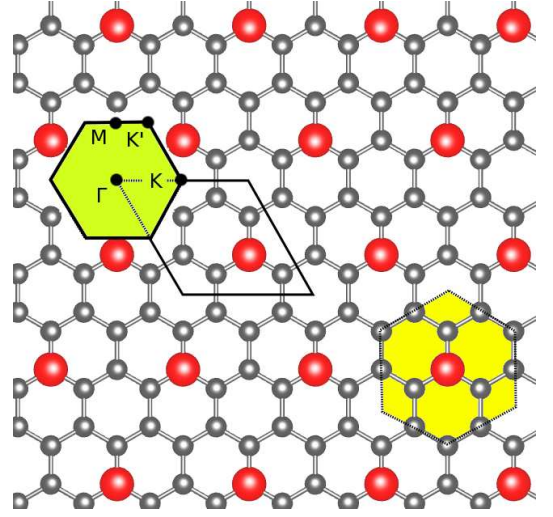


Figure 4: A 2x2-hexagon superlattice: the black line represents the unit cell boundary while the Wigner-Seitz and Brillouin zone are filled in yellow and green respectively. Red balls are substitutional defects positions.

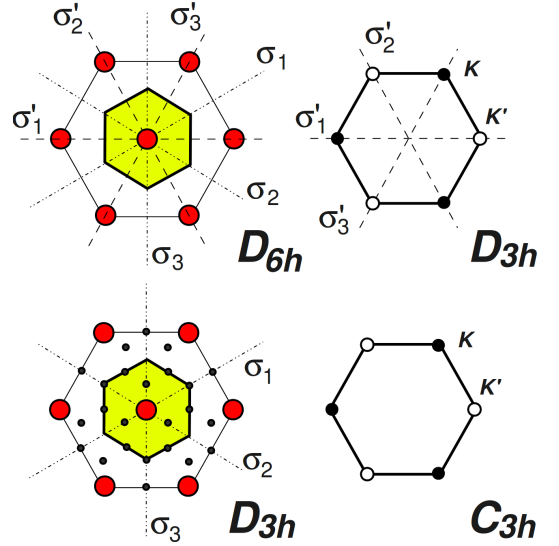


Figure 5: Wigner-Seitz (yellow, left side) and Brillouin zone (right side) for the hexagonal superlattices. Considering the defects only the point group is D_{6h} , and the corresponding k -group in K_n D_{3h} (upper panel). Overall the underlying carbons remove the σ' planes, reducing the symmetry to D_{3h} .

moved at the special points and a (small) gap opens in the band structures, close to the (shifted) Fermi energy. This is shown in 6(a) where the TB and DFT band-structures of the 4x4 hexagon are reported. The energy spectrum of such gapped graphene is compatible with charge carriers behaving as *massive* Dirac particles

$$E(\mathbf{k}) = \pm v \sqrt{k_x^2 + k_y^2 + m^2 v^2} \quad (1)$$

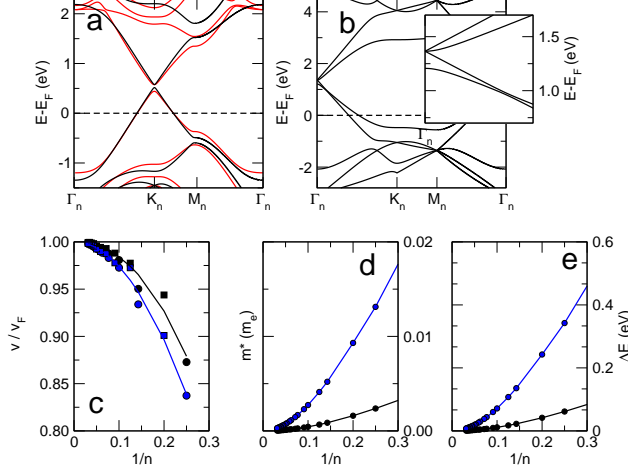


Figure 6: *a)* TB (black) and DFT (red) band structures for the 4x4-hexagon. *b)* the TB band structure of the 3x3-hexagon boron superlattice arising from folding in $n = 3m$ superlattices. The inset shows a close-up of the region close to Γ_n . Carriers effective speeds (c), masses (d) and energy band-gaps (e) versus $1/n$. Black and blue values refer to B and N superlattices, respectively.

where v, m^* are the effective ‘speed of light’ and ‘rest mass’, respectively, and determine the gap size

$$\Delta E = 2m^*v^2 \quad (2)$$

According to the semiclassical theory of conduction m^* is also the effective mass m_{eff} governing charge carrier mobility for $k \ll mv$; for $k \gg mv$ carriers behave pseudorelativistically with $m_{eff} = 0$ and limiting speed v . The values v, m^* and ΔE have been obtained by non-linear curve fitting of the numerical results to 1 and are reported in panels (b)-(d) of 6. For nxn -hexagons the band gap is very dependent on the type of dopant (6.e): the maximum gaps, occurring in 2x2 hexagons, are 0.93 eV for nitrogen and only 0.17 eV for boron. The effective masses of electrons and holes (6.d)) roughly scale as the gaps: $\propto n^{-1.45}$ and $\propto n^{-1.52}$ for n - and p -doped structures respectively, and their maximum is 3.7×10^{-2} and $6.7 \times 10^{-3} m_e$. This is similar to the case of graphene nanoribbon⁴⁰, whose band gap scales as the inverse of their width even though here the gap is due to symmetry breaking rather than quantum confinement. The shift of the Fermi level (not shown) is again proportional to the square root of the defects concentration, that is now only half of the value for honeycombs with the same superlattice periodicity. Charge carriers velocities scale similarly for the two dopant species as shown in 6.(c) with a best-fit exponent close to -2 ($v(B)/v_F \propto 1 - n^{-1.98}$, $v(N)/v_F \propto 1 - n^{-2.28}$). In 6, panel (b), we also report the particular band structure arising in $n = 3m$ hexagon superlattices. At the relevant special point Γ_n ,

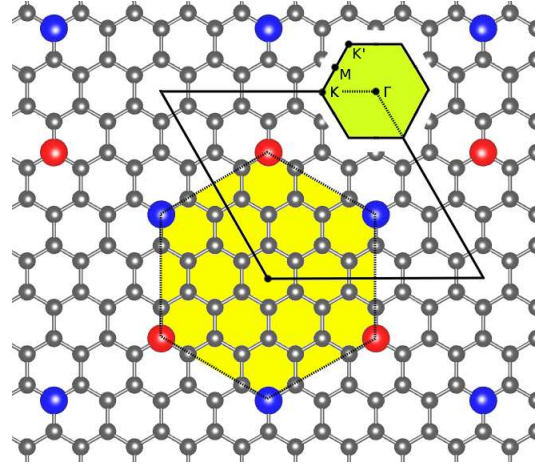


Figure 7: A 4x4-honeycomb superlattice: the black line represents the unit cell while the Wigner-Seitz and Brillouin zone are shown in yellow and green respectively. Red and Blue balls are B and N substitutional defects.

the massive, pseudo-relativistic energy dispersion is superimposed with a massless one, thereby giving rise to a two-valley system with very different charge carriers. As shown in the next subsection, all the features discussed in this Section can be brought at the Fermi level by co-doping the substrate in forming a honeycomb structure with the same D_{3h} symmetry discussed here.

C. Co-doped superlattices

One further possible superlattice arrangement is obtained by using two different dopants in the nxn -honeycomb unit cell, *i.e.* co-doping the structures with boron and nitrogen (see 7). In this way B and N atoms form a boron nitride-like honeycomb superlattice in which sublattices equivalence (and symmetry) is broken. This is analogous to place graphene in the modulating field of a proper substrate, *e.g.* a hexagonal BN (0001) surface, which has been shown to lift the degeneracy of the $\pi - \pi^*$ bands⁴¹; similarly for deposition, or growth, on silicon carbide surfaces^{42,43}. The superlattice structures considered here offer the possibility to modify the periodicity of the perturbation, and thus to tune the gap. Indeed, this kind of superlattices present D_{3h} point symmetry, hence a C_{3h} k -group in K_n, K'_n , and, analogously to the hexagonal case discussed above, open a band gap typical of massive Dirac particles. Differently from before, however, the structures considered here are iso-electronic with graphene and therefore the gap lies exactly at the Fermi energy. 8 shows the computed band structure (panel (a)), together with the values of the effective speed of light (c), effective mass (d) and band gaps (e), obtained as in previous section by fitting of the numerical results, for different BN nxn -honeycombs. The results confirm the expectations, and show that such structures present a band-gap at the Fermi energy, com-

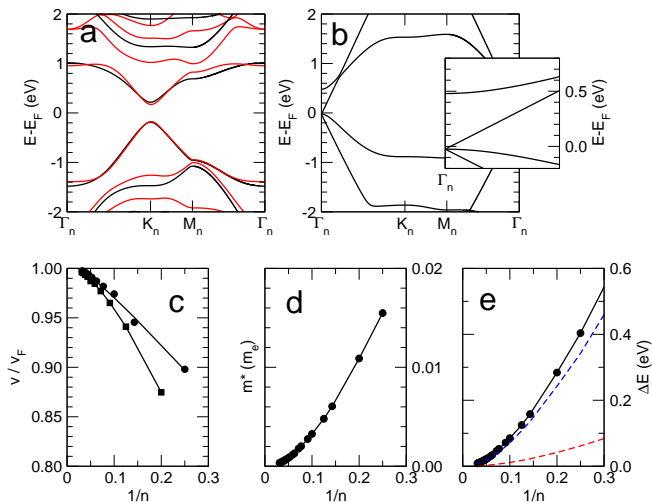


Figure 8: a) TB and DFT band structures for the co-doped 4x4-honeycomb. b) the case of 3x3 superlattice with the low-energy region in the inset. c) Effective speed, d) mass at the K_n point versus $1/n$, and e) band-gap. The red and the blue dashed lines are the values for n - and p -doped hexagons, shown for comparison.

patible with pseudo-relativistic massive carriers. Their effective rest mass is rather small, scales as $\propto n^{-1.46}$ and it is never larger than $0.016 m_e$ for $n \geq 4$. This value compares favorably with the effective masses in $\text{Bi}_{1-x}\text{Sb}_x$ topological insulators ($m^*=0.009 m_e$)⁴⁴, and is generally lower than in bilayer graphene ($m^*=0.03 m_e$)⁴⁵ or in any other traditional bulk semiconductors, such as InSb ($m^*=0.016 m_e$). Since m^* is the main factor affecting carrier mobility, the suggested structures turn out to be a good compromise between the need of opening a gap for logic applications and the desire of preserving the high mobility of charge carriers. In 8, panel (b) we also report the band structure of the $n = 3m$ case. The structure is that of a zero-gap semiconductor, with two distinct charge carriers: one of them behave as electron (hole) in graphene, showing typical effects expected for massless carriers; the other is a more conventional one, with a finite excitation energy across a gap.

IV. SUMMARY AND CONCLUSIONS

To summarize, we have studied the effects substitutional defects such B and N species have on graphene electronic structure when they are periodically arranged to form some superlattices. Using group theoretical arguments and both TB and DFT calculations we have shown that defects can either preserve the Dirac cones or open a band gap, depending on the superlattice symmetry (D_{6h} and D_{3h} , respectively). Specifically, honeycomb-shaped superlattices of B or N atoms give rise to p - and n -doped graphene, respectively, preserving the Dirac cones. On the other hand, when a hexagonal superlattice is formed,

or the honeycomb one is symmetrically co-doped, the Dirac cones detach from each other to form a gapped, quasi-conical structure whose excitations correspond to massive Dirac particles. Note that this situation clearly differs from the case of randomly arranged B or N impurities, in which the density of states shows no band gap³⁶.

For zero-gap structures the use of this superlattices offers the possibility to control the Fermi velocity by changing the structure periodicity, thereby offering the opportunity to investigate its role in the charge transport properties. Differently from our recent proposal²¹, the gapped band structures arise because of symmetry breaking, as in the case of graphene interacting with a substrate such as SiC or BN. In the same fashion the band gap size depends on the superlattice periodicity. In our calculations we have found that gaps and charge carriers velocities effective masses depends on $1/n^p$, where p is in the range $1 - 2$, hence on some small power $0.5 - 1$ of the dopant concentration, and on the dopant type (B or N). Overall the structures proposed here show a band gap larger than $k_B T$ at room temperature, with an effective mass generally lower than $0.01 m_e$ for reasonably dense meshes ($n=4-10$). Thus, the new class of graphene structures proposed might be promising candidates for the fabrication of high performance interconnects, valley-based devices⁴⁶, but also for logic transistors, where a band gap is needed, but the extraordinary properties of pristine graphene need to be preserved.

The electronic properties of these impurities superlattices rely on symmetry, hence are necessarily sensitive to the dopant positions. As a consequence, an accurate control of the system geometry is necessary to exploit their properties. This might be possible in the near future with precise bottom-up techniques, such as the ones recently used by Ruffieux and co-workers^{19,20} to fabricate nanoribbons of well-defined widths and edges. An indication of the possible synthetic routes together with formation energies for such defects superlattices can be found in the Supporting Information. This information is available free of charge via the Internet at <http://pubs.acs.org>.

V. SUPPORTING INFORMATION

In order to compare relative structural stabilities, formation energies for superlattice structures have been computed as follows:

$$\Delta H_{form} = E_{SL} - (2n^2 - \eta)\mu_C - n_N\mu_N - n_B\mu_B \quad (3)$$

where E_{SL} is the total energy of the structure, n is the superlattice constant, η is the number of dopants per cell (1 for hexagons and 2 for honeycombs), n_i and μ_i are the number of atoms and the chemical potentials for each species. The chemical potentials were computed with respect to single layer graphene, gaseous N_2 and α -Boron (in the so-called R12 structure). Density functional the-

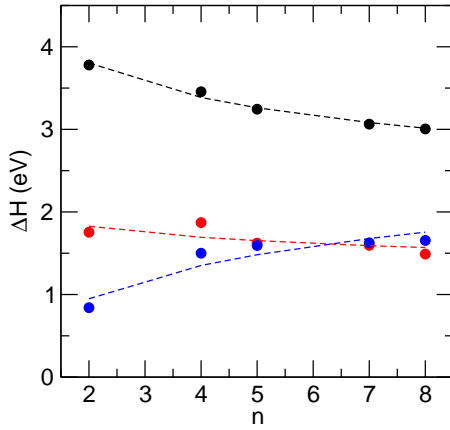


Figure 9: DFT formation enthalpies (in eV) for Boron (black), Nitrogen (red) and co-doped (blue) honeycombs. Dashed lines show non-linear fits as a guide for the eye

Table II: DFT formation enthalpies for doped superlattices for structures up to $n=8$ arranged by doping and by superlattice symmetry. All the values shown are in eV

n	Hexagon		Honeycomb		
	B	N	B	N	BN
2	1.840	1.078	3.780	1.754	0.841
4	1.513	0.878	3.455	1.871	1.500
5	1.499	0.933	3.224	1.622	1.593
7	1.380	0.676	3.063	1.596	1.626
8	1.394	0.695	3.005	1.490	2.023

ory results are shown in II and in figure 9.

For all the cases considered the formation energy of the superlattice structures is endothermic with respect to the pure elements with opposite trends for n - (p -)doped and co-doped structures. While two impurities of the same kind gain energy when lying further apart to each other, B and N tend instead to cluster together, in accordance with recent experimental observations²⁸. However, in order to cluster the impurities have to diffuse through the graphene lattice by exchanging its position with a carbon atom. Such a process has a large energetic barrier being the two atoms covalently bound, hence the kinetics of this process is expected to be extremely slow. We therefore suggest that these structures are expected to be stable at room temperature as well as other known structures (*e.g.* graphene itself with respect to diamond).

About the practical feasibility of substitutional defects superlattices we expect they can be produced by the same bottom-up approach recently used to fabricate graphene structures with atomic-scale control^{19,20}. According to this method an appropriate polyphenylene precursor, *e.g.* produced by Ullmann coupling, undergo cyclodehydrogenation on a Cu surface to form a polycyclic aromatic hydrocarbon (PAH)^{47–50}, that in our case should include the dopant atom. When appropriately functionalized the PAHs can then polymerize on the metal surface to form graphene domains up to a nanometer scale as recently shown for the synthesis of the atomically precise nanoribbons²⁰. Such a technique has been also adopted to produce nitrogen doped fullerenes⁵¹ and two-dimensional polymers⁵², hence it might indeed lead to graphene-based superlattices of substitutional defects starting from chemically doped polycyclic aromatic hydrocarbons.

* Electronic address: simone.casolo@unimi.it; Electronic address: rocco.martinazzo@unimi.it

¹ Slonczewski, J. C.; Weiss, P. R. *Phys. Rev.* **1958**, *109*, 272.

² Castro Neto, A. H.; Guinea, F.; Peres, N. M. R.; Novoselov, K. S.; Geim, A. K. *Rev. Mod. Phys.* **2009**, *81*, 109.

³ Abergel, D. S. L.; Apalkov, V.; Berashevich, J.; Ziegler, K.; Chakraborty, T. *Adv. Phys.* **2010**, *59*, 261.

⁴ Schwierz, F. *Nature Nanotech.* **2010**, *5*, 487.

⁵ Lin, Y.-M.; Jenkins, K. A.; A. Valdes-Garcia, J. P. S.; Farmer, D. B.; Avouris, P. *Nano. Lett.* **2009**, *9*, 422.

⁶ Avouris, P. *Nano. Lett.* **2010**, *10*, 4285.

⁷ Peres, N. M. R. *Rev. Mod. Phys.* **2010**, *82*, 2673.

⁸ Avouris, P.; Chen, Z.; Perebeinos, V. *Nat. Nanotech.* **2007**, *2*, 605.

⁹ Tiwari, R. P.; Stroud, D. *Phys. Rev. B* **2009**, *79*, 205435.

¹⁰ Park, C.; Yang, L.; Son, Y.; Cohen, M. L.; Louie, S. G. *Phys. Rev. Lett.* **2008**, *101*, 126804.

¹¹ Pedersen, T. G.; Flindt, C.; Pedersen, J.; Mortensen, N. A.; Jauho, A.; Pedersen, K. *Phys. Rev. Lett.* **2008**, *100*, 136804.

¹² Liu, W.; Zhang, Z. F.; Shi, Q. W.; Yang, J.; Liu, F. *Phys. Rev. B* **2009**, *80*, 233405.

¹³ Chernozatonskii, L. A.; Sorokin, P. B. *J. Phys. Chem. C* **2010**, *114*, 3225.

¹⁴ Fischbein, M.; Drnić, M. *Appl. Phys. Lett.* **2008**, *93*, 113107.

¹⁵ Bai, J. W.; Zhong, X.; Jiang, S.; Y, Y. H.; Duan, X. F. *Nature Nanotech.* **2010**, *5*, 190.

¹⁶ Balog, R. et al. *Nat. Mater.* **2010**, *4*, 315.

¹⁷ Cheianov, V. V.; Syljuåsen, O.; Altshuler, B. L.; Fal'ko, V. *Phys. Rev. B* **2009**, *80*, 233409.

¹⁸ Cheianov, V. V.; Syljuåsen, O.; Altshuler, B. L.; Fal'ko, V. *Europhys. Lett.* **2010**, *89*, 56003.

¹⁹ Bieri, M.; Treier, M.; Cai, J.; Ait-Mansour, K.; Ruffieux, P.; Gröning, O.; Gröning, P.; Kastler, M.; Rieger, R.; Feng, X.; Müllen, K.; Fasel, R. *Chem. Comm.* **2009**, *45*, 470.

²⁰ Cai, J.; Ruffieux, P.; Jaafar, R.; Bieri, M.; Braun, T.; Blankenburg, S.; Muoth, M.; Seitsonen, A.; Saleh, M.; Feng, X.; Müllen, K.; Fasel, R. *Nature* **2010**, *466*, 470.

²¹ Martinazzo, R.; Casolo, S.; Tantardini, G. F. *Phys. Rev. B*

- 2010, *81*, 245420.
- ²² Dutta, S.; Manna, A. K.; Pati, S. K. *Phys. Rev. Lett.* **2009**, *102*, 0966011.
 - ²³ Dutta, S.; Pati, S. K. *J. Phys. Chem. B* **2008**, *112*, 1333.
 - ²⁴ Zheng, X. H.; Wang, X. L.; Abtew, T. A.; Zeng, Z. *J. Phys. Chem. C* **2010**, *114*, 4190.
 - ²⁵ Yu, S. S.; Zheng, W. T. *Nanoscale* **2010**, *2*, 1069.
 - ²⁶ Dutta, S.; Pati, S. K. *J. Mater. Chem.* **2010**, *20*, 8207.
 - ²⁷ Panchakarla, L. S.; Subrahmanyam, K. S.; Saha, S.; Govindaraj, A.; Krishnamurthy, H. R.; Waghmare, U. V.; Rao, C. N. R. *Adv. Mater.* **2009**, *21*, 4726.
 - ²⁸ Ci, L.; Song, L.; Jin, C.; Jariwala, D.; Wu, D.; Li, Y.; Srivastava, A.; Wang, Z. F.; Storr, K.; Balicas, L.; Liu, F.; Ajayan, P. M. *Nature Mater.* **2010**, *9*, 430.
 - ²⁹ Pontes, R. B.; Fazzio, A.; Dalpian, G. M. *Phys. Rev. B* **2009**, *79*, 033412.
 - ³⁰ Nanda, B. R. K.; Satpathy, S. *Phys. Rev. B* **2009**, *80*, 165430.
 - ³¹ Peres, N. M. R.; Klironomos, F. D.; Tsai, S. W.; Santos, J. R.; Lopes dos Santos, J. M. B.; Castro Neto, A. H. *Europhys. Lett.* **2007**, *80*, 67007.
 - ³² Kresse, G.; Hafner, J. *Phys. Rev. B* **1994**, *49*, 14251.
 - ³³ Kresse, G.; Hafner, J. *Phys. Rev. B* **1993**, *47*, 558.
 - ³⁴ Perdew, J. P.; Burke, K.; Ernzerhof, M. *Phys. Rev. Lett.* **1996**, *77*, 3865.
 - ³⁵ Mirman, R. *Point groups, space groups, crystals and molecules*; World Scientific, 1999.
 - ³⁶ Lherbier, A.; Blase, X.; Niquet, Y.; Triozon, F.; Roche, S. *Phys. Rev. Lett.* **2008**, *101*, 036808.
 - ³⁷ Zheng, B.; Hermet, P.; Hernard, L. *ACS Nano* **2010**, *4*, 4165.
 - ³⁸ Coletti, C.; Riedl, C.; Lee, D. S.; Krauss, B.; Patthey, L.; von Klitzing, K.; Smet, J. H.; Starke, U. *Phys. Rev. B* **2010**, *81*, 235401.
 - ³⁹ Pinto, H.; Jones, R.; Goss, J. P.; Briddon, P. R. *Phys. Stat. Sol. A* **2010**, *207*, 2131.
 - ⁴⁰ Barone, V.; Hod, O.; Scuseria, G. *Nano. Lett.* **2006**, *6*, 2748.
 - ⁴¹ Giovannetti, G.; Khomyakov, P. A.; Brocks, G.; Kelly, P. J.; van der Brink, J. *Phys. Rev. B* **2007**, *76*, 073103.
 - ⁴² Mattausch, A.; Pankratov, O. *Phys. Rev. Lett.* **2007**, *99*, 076802.
 - ⁴³ Varchon, F.; Feng, R.; Li, X.; Ngoc Nguyen, B.; Naud, C.; Veullien, J. Y.; Berger, C. *Phys. Rev. Lett.* **2007**, *99*, 126805.
 - ⁴⁴ Hsieh, D.; Qian, D.; Wray, L.; Xia, Y.; Hor, Y.; Cava, R.; Hasan, M. *Nature* **2008**, *452*, 970.
 - ⁴⁵ Castro, E. V.; Peres, N.; Lopes do Santos, J.; Guinea, F.; Castro Neto, A. *J. Phys.: Conf. Ser.* **2008**, *129*, 012002.
 - ⁴⁶ Xiao, D.; Yao, W.; Niu, Q. *Phys. Rev. Lett.* **2007**, *99*, 236809.
 - ⁴⁷ Weiss, K.; Beernink, G.; Dötz, F.; Birkner, A.; Müllen, K.; Wöll, C. *Angew. Chem. Int. Ed.* **1999**, *38*, 3748.
 - ⁴⁸ Beernink, G.; Gunia, M.; Dötz, F.; Öström, H.; Weiss, K.; Müllen, K.; Wöll, C. *ChemPhysChem* **2001**, *2*, 317.
 - ⁴⁹ Lipton-Duffin, J. A.; Ivashenko, O.; Perepichka, D. F.; Rosei, F. *Small* **2009**, *5*, 592.
 - ⁵⁰ Treier, M.; Pignedoli, C. A.; Laino, T.; Rieger, R.; Müllen, K.; Passerone, D.; Fasel, R. *Nat. Chem.* **2010**, in press, doi:10.1038/nchem.891.
 - ⁵¹ Otero, G.; Biddau, G.; Snchez-Snchez, C.; Caillard, R.; Lpez, M. F.; Rogero, C.; Palomares, F. J.; Cabello, N.; Basanta, M. A.; Ortega, J.; Mndez, J.; Echavarren, A. M.; Prez, R.; Gmez-Lor, B.; Martn-Gago, J. A. *Nature* **2008**, *454*, 865.
 - ⁵² Treier, M.; Richardson, N. V.; Fasel, R. *J. Am. Chem. Soc.* **2008**, *130*, 14054.
 - ⁵³ Notice that even though $e - h$ symmetry only holds in the nearest neighbors approximation and in absence of diagonal disorder, the Fermi level always matches the doubly degenerate state at K (K') as long as the $e - h$ symmetry breaking does not cause the maximum (minimum) of the valence (conduction) band to exceed the energy at K .